Effect of Measurement Errors On Master Plane Representations of Target Position in an Air Traffic Control System

R. G. Mulholland
D. W. Stout

December 1982

DOT/FAA/CT-81/48

U.S. Department of Transportation
Federal Aviation Administration

Technical Center
Atlantic City Airport, N.J. 08405

NOTICE

This document is disseminated under the sponsorship of the Department of Transportation in the interest of information exchange. The United States Government assumes no liability for the contents or use thereof.

The United States Government does not endorse products or manufacturers. Trade or manufacturer's names appear herein solely because they are considered essential to the object of this report.

Technical Report Documentation Page

1. Report No.	2. Government Accession No.	3. Recipient's Catalog No.
DOT/FAA/CT-81/48		

4. Title and Subtitle	5. Report Date
EFFECT OF MEASUREMENT ERRORS ON MASTER PLANE REPRESENTATIONS OF TARGET POSITION IN AN AIR TRAFFIC CONTROL SYSTEM	December 1982
	6. Performing Organization Code
7. Author(s) R. G. Mulholland, D. W. Stout	8. Performing Organization Report No. DOT/FAA/CT-81/48
9. Performing Organization Name and Address Federal Aviation Administration Technical Center Atlantic City Airport, N. J. 08405	10. Work Unit No. (TRAIS) 11. Contract or Grant No. 975-200-10A
12. Sponsoring Agency Name and Address U.S. Department of Transportation Federal Aviation Administration Technical Center Atlantic City Airport, N. J. 08405	13. Type of Report and Period Covered Final October 1980 14. Sponsoring Agency Code

15. Supplementary Notes

16. Abstract

This report deals with formulations of the effects of errors in the measurement of slant range, azimuth, and altitude on master plane representations of target position in an air traffic control system supported by a multitude of surveillance radars. It is concerned with the case in which such representations are based on the method of stereographic projection. Special consideration is afforded the statistical characterization of fluctuations induced in the master plane by random measurement errors, and to confidence regions for target location that might be useful in the automatic tracking of aircraft. Emphasis is placed on noise levels commonly associated with Mode S and the Air Traffic Control Radar Beacon System (ATCRBS) under constraints consistent with the structure of coverage regions of domestic Air Route Traffic Control Centers (ARTCC's).

17. Key Words		18. Distribution Statement
Altitude	Local Plane	
Slant Range	Planar Representation	
Azimuth	Ellipsoid	
Stereographic Projection	Master Plane	
Orthogonal Projection		

19. Security Classif. (of this report)	20. Security Classif. (of this page)	21. No. of Pages	22. Price
Unclassified	Unclassified	32	

METRIC CONVERSION FACTORS

Approximate Conversions to Metric Measures

Symbol	When You Know	Multiply by	To Find	Symbol
	LENGTH			
in	inches	*2.5	centimeters	cm
ft	feet	30	centimeters	cm
yd	yards	0.9	meters	m
mi	miles	1.6	kilometers	km
	AREA			
in^2	square inches	6.5	square centimeters	cm^2
ft^2	square feet	0.09	square meters	m^2
yd^2	square yards	0.8	square meters	m^2
mi^2	square miles	2.6	square kilometers	km^2
	acres	0.4	hectares	ha
	MASS (weight)			
oz	ounces	28	grams	g
lb	pounds	0.45	kilograms	kg
	short tons (2000 lb)	0.9	tonnes	t
	VOLUME			
tsp	teaspoons	5	milliliters	ml
Tbsp	tablespoons	15	milliliters	ml
fl oz	fluid ounces	30	milliliters	ml
c	cups	0.24	liters	l
pt	pints	0.47	liters	l
qt	quarts	0.95	liters	l
gal	gallons	3.8	liters	l
ft^3	cubic feet	0.03	cubic meters	m^3
yd^3	cubic yards	0.76	cubic meters	m^3
	TEMPERATURE (exact)			
°F	Fahrenheit temperature	5/9 (after subtracting 32)	Celsius temperature	°C

*1 in = 2.54 (exactly). For other exact conversions and more detailed tables, see NBS Misc. Publ. 286, Units of Weights and Measures, Price $2.25, SD Catalog No. C13.10:286.

Approximate Conversions from Metric Measures

Symbol	When You Know	Multiply by	To Find	Symbol
	LENGTH			
mm	millimeters	0.04	inches	in
cm	centimeters	0.4	inches	in
m	meters	3.3	feet	ft
m	meters	1.1	yards	yd
km	kilometers	0.6	miles	mi
	AREA			
cm^2	square centimeters	0.16	square inches	in^2
m^2	square meters	1.2	square yards	yd^2
km^2	square kilometers	0.4	square miles	mi^2
ha	hectares (10,000 m^2)	2.5	acres	
	MASS (weight)			
g	grams	0.035	ounces	oz
kg	kilograms	2.2	pounds	lb
t	tonnes (1000 kg)	1.1	short tons	
	VOLUME			
ml	milliliters	0.03	fluid ounces	fl oz
l	liters	2.1	pints	pt
l	liters	1.06	quarts	qt
l	liters	0.26	gallons	gal
m^3	cubic meters	35	cubic feet	ft^3
m^3	cubic meters	1.3	cubic yards	yd^3
	TEMPERATURE (exact)			
°C	Celsius temperature	9/5 (then add 32)	Fahrenheit temperature	°F

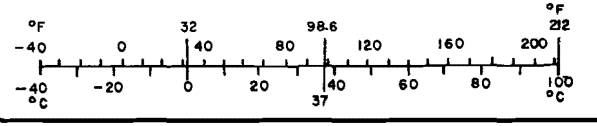

TABLE OF CONTENTS

LIST OF ILLUSTRATIONS

EXECUTIVE SUMMARY

At an Air Route Traffic Control Center (ARTCC), horizontal separation of aircraft is based on estimates of current and future positions as provided by automatic tracking filters. Tracker input data are obtained by means of a series of arithmetic operations on the measurement of slant range, azimuth, and altitude to form a two-dimensional representations of target position. Tracking performance, and, hence, maintenance of the horizontal separation standards, is a function of the statistical quality of the tracker input data. This, in turn, is dependent upon the measurement accuracy of the sensor and the method used to convert target radar coordinates into a two-dimensional point. Accordingly, this report deals with the interdependent relationship between measurement errors and distortions in the representations of target position. In addition, consideration is afforded the statistical characterization of errors which must be known in order to evaluate tracker performance in an Air Traffic Control Radar Beacon System (ATCRBS) or a Mode S sensor environment.

1. INTRODUCTION

This report deals with linear formulations of the effect of measurement errors in the planar representation of targets in multiple radar surveillance systems in the domestic en route air traffic control (ATC) environment. Specifically, it pertains to those instances where such representations are derived via a two-stage procedure based on the method of stereographic projection (reference 1). The first stage involves a conversion of reported altitude, measured target slant range, and measured azimuth (measurements relative to a specific radar site) into a point on a local radar plane. The second stage involves a transformation to carry points in the local plane into a single, master plane. Every local plane corresponds to a radar, and each is mapped onto the master plane to establish the final planar representation of target positions within the coverage region of the surveillance system.

Section 2 summarizes some parameter constraints that are consistent with the operation of an ARTCC. Section 3 reviews formulas by which measurements of target position can be mapped into the master plane in such multiple radar data processing systems. Consideration is given to both a minimax and a correction technique for controlling the so-called conversion error. Section 4 treats several types of measurement errors. Approximations for analyzing the effect of such errors on the representation of targets in the master plane are described in section 5. In section 6, these approximations are used to derive the second moments of fluctuations in the master plane due to random measurement errors. Section 7 is concerned with the design of elliptical confidence regions for the master plane image of actual target position under the two-stage conversion and transformation procedure. Concluding remarks appear in section 8.

2. CONSTRAINTS ON SLANT RANGE AND ALTITUDE

This section deals with the location of geophysical points relative to the reference ellipsoid (reference 1). This is an ellipsoid of revolution with semimajor and semiminor axes

$$a = 3444.0540 \text{ nmi and } b = 3432.4579 \text{ nmi}$$

that closely approximates the equipotential surface of gravity at mean sea level. By altitude, we mean altitude above mean sea level, or equivalently, the distance between a point and its orthogonal projection onto the reference ellipsoid. In particular, we will be concerned with a radar site located at an altitude H_R above a point on the ellipsoid that is removed a distance E_S from its geometric center.

Radar measurements of the positions of a point target consist of the reported target altitude, H, an observed target slant range, S, and an observed target azimuth, θ. In the absence of a measurement error, H is the altitude of the target above mean sea level, S is the distance between the radar site and the target, and θ is the angle in the radar platform plane measured in the direction of platform rotation from the plane passing through the polar axis of the ellipsoid and the meridian defining the longitude of the radar site.

Some combinations of reported altitude and slant range measurement are unacceptable. For example, admissible values of S are limited by both the radar's maximum effective range S_M and its minimum range S_m (due to interference phenomena). In addition, the altitude, H, of targets of interest is assumed as limited by some constant H_M. Moreover, the radar cone of silence constrains the ratio $|H - H_R|$ to S below some constant J. Thus, S and H are restricted by the following inequalities in practical application:

$$0 < S_m \leq S \leq S_M \qquad |H - H_R|/S \leq J \qquad 0 \leq H \leq H_M \tag{1}$$

In this paper, it is assumed that: (1 m = 0.3048 ft and 1 nmi = 1,852 m).

$$S_M = 200 \text{ nmi}, \qquad S_m = 2 \text{ nmi}, \qquad J = \sin 70°.$$

This assumption is consistent with the current operation of ARTCC's within the National Airspace System (NAS) as well as existing specifications concerning future sensor enhancement through the introduction of Mode S. Moreover, since controlled traffic consists mainly of aircraft at altitudes less than 60,000 feet, we will assume that:

$$H_M = 9.88 \text{ nmi}$$

Finally, we will refer to the vector (S,H) as an admissible point only if it satisfies the constraints (1). Thus, admissibility is compatible with requirements governing the utility of reported altitude and slant range measurement to the control function under typical operating conditions in the en route environment, both now and in the forseeable future.

Since all NAS radar site altitudes are below 10,000 feet sea level, H_R can be considered to be constrained by the inequality:

$$0 \leq H_R \leq 1.646 \text{ nmi}$$

3. COMPLEX REPRESENTATIONS OF TARGET POSITION

The corrected slant range defined by:

$$R(S,H) = [S^2 - (H - H_R)^2]^{1/2} \tag{2}$$

is of fundamental importance in the formation of planar representations of the datum (S,θ, H). In particular, the datum is mapped into a point on the so-called local radar plane represented by the complex number:

$$z(\rho,\theta) = \rho\epsilon^{i\left(\frac{\pi}{2} - \theta\right)} \tag{3}$$

where ρ is a function of the reported altitude and the product of R and a parameter, α, defined by:

$$\alpha(E_S,H_R)^{-1} = [([1 + (H_R + H_M)/E_S + H_R H_M/E_S^2]^{1/3} + [1 + H_R/E_S]^{2/3})/2]^{3/2} \quad (4)$$

The relationship between ρ, H, and αR depends on the method used to control the conversion error. For example, in the minimax method currently employed in NAS, the relationship is expressed as:

$$\rho(\alpha R,H) = \alpha R \quad (5)$$

In the error correction method introduced in (reference 1), it is:

$$\rho(\alpha R,H) = 2\alpha R - \alpha R[1 + K/b]^{-1/2} [1 + H/2b - \alpha^2 R^2/8b^2] \quad (6)$$

where:

$$K = 10.039 \text{ nmi } (61{,}000 \text{ ft})$$

In either case, ρ can be considered an approximate measure of the distance between the orthogonal projections of the radar site and the target on the reference ellipsoid.

Unfortunately, the effective range of a single radar is not sufficient to cover the airspace under the control of an ARTCC. Consequently, representations of the type (3) cannot, by themselves, provide a meaningful measure of the overall spatial relationship between targets. However, it is possible to map the elements of each local radar plane onto a single master plane so that the images of elements in two or more local planes corresponding to the same target, or several targets with identical latitude and longitude but different altitudes, are essentially the same (in fact, they are the same in the absence of measurement error and conversion error). This is accomplished by the bilinear transformation (reference 1):

$$w(z) = [w_o + (E_r/E_s)\, z\epsilon^{-i\beta}][\, 1 - z(4E_rE_s)^{-1}w_o^*\, \epsilon^{-i\beta}]^{-1} \quad (7)$$

where w_o, is the image of the radar site, w_o^* is the complex conjugate of w_o, E_r is the radius of the so-called conformal sphere that supports the master plane, and β is an angle determined by both the latitude and longitude coordinates of the radar site and those selected for the point of tangency where the master plane and its spherical support meet.

Discounting measurement conversion error (reference 1), the resultant representations based on equations (3) and (7) are identical.

4. MEASUREMENT ERRORS

In practice, some difference is expected between the actual position of the target and its positional measurement derived via observation at the radar site. Thus, the measured vectoral position (S,θ,H) can be incremented by ΔS, $\Delta\theta$, and ΔH so that $(S + \Delta S, \theta + \Delta\theta, H + \Delta H)$ represents the actual location of the target in terms

of slant range, azimuth, and altitude above mean sea level. In this sense, the vector $(\Delta S, \Delta\theta, \Delta H)$ represents the measurement error.

Two types of errors that arise in a series of consecutive observations of any one of the three coordinates of target position will be considered. First, there is an error due to stochastic phenomena such as thermal noise in the components of the radar receiver. These random errors can vary widely from observation to observation, and they are often treated as a sequence of independent and identically distributed stochastic variables with zero mean and finite variance. The second type of error can be conceived as a signal of very low frequency relative to the observation rate and it can often be effectively modelled as a constant over many consecutive observations.

Apparently, little effort has been expended to quantitatively characterize the difference between reported altitude and the actual altitude of the target above mean sea level. However, reports from a variety of aircraft have been compared with those from a reference aircraft using the so-called pacer method, and a recent investigation (reference 2) indicates an upper bound of 0.0183 nmi for the standard deviation of the random altitude error. Moreover, in a comparison (reference 3) between assigned flight levels of 31 commercial aircraft and high precision radar measurements of geometric altitude, average altitude differences were less than 1,200 feet. This, of course, cannot be construed as conclusive evidence that altitude bias errors rarely exceed 1,200 feet or any other prescribed level. Nevertheless, since it is the only data base currently available, the scope of this study will be restricted to those cases where $|\Delta H|$ is less than 0.329 nmi (2,000 feet).

A real time quality control (RTQC) system within NAS provides estimates of bias errors in slant range and azimuth. These estimates are used to adjust the sensor system to minimize such biases. In all but extreme cases, RTQC should detect and eliminate a bias error before it can exceed three standard deviations of the random error in the same coordinate. The standard deviations of random errors in slant range and azimuth exhibited in table 1 are representative of sensor measurement accuracies in Mode S and the current ATCRBS. Evidently, a bias error in slant range (azimuth) exceeding 0.375 nmi (0.0138) rad is unlikely to occur in the presence of an adequate RTQC function.

TABLE 1. STANDARD DEVIATION OF RANDOM ERRORS

	STANDARD DEVIATION	
SENSOR:	Slant Range	Azimuth
ATCRBS	1.25×10^{-1} nmi	4.60×10^{-3} rad
Mode S	8.23×10^{-3} nmi	1.75×10^{-3} rad

In view of the preceding observations, the following examples would seem to represent fairly realistic situations of frequent occurrence and practical import. A simple, linear approximation of the complex, interrelation between the error $(\Delta S, \Delta\theta, \Delta H)$ and the corresponding difference between the representations of (S,θ,H) and $(S + \Delta S, \theta + \Delta\theta, H + \Delta H)$ in the master plane is useful in expediting the analyses in the following examples:

Example 1: The datum (S,θ,H) is acquired through an ATCRBS radar. As a result of RTQC, the bias errors in slant range and azimuth are negligible. In addition, $|\Delta S| \leq 0.375$ nmi, $|\Delta\theta| \leq 0.0138$ rad, and $|\Delta H| \leq 0.329$ nmi. Moreover, (S,H) is an admissible point for which:

$$|H - H_R| \leq [S(S - 2k)]^{1/2} \tag{8}$$

where k is 4.13, i.e., the measured position of the target is not too close to the radar as illustrated in figure 1 (also see appendix A).

Example 2: The situation is identical to that of example 1 except that the radar is a Mode S sensor, $|\Delta S| \leq 0.0247$ nmi, $|\Delta\theta| \leq 0.00525$ rad, and k = 1.98.

Example 3: The RTQC subsystem is operating in an environment where the errors satisfy the inequalities $|\Delta S| \leq 1$ nmi, $|\Delta\theta| \leq 0.03$ rad, and $|\Delta H| \leq 0.329$ nmi. Any datum (S,θ,H) used for estimation must be such that (S,H) is an admissible point and S cannot be less than 20 nmi.

5. APPROXIMATIONS

The increment:

$$\Delta R = R(S + \Delta S, H + \Delta H) - R(S,H) \tag{9}$$

can be expressed as:

$$\Delta R = [S/R(S,H)]g(1 + \eta_1) \tag{10}$$

where:

$$g = \Delta S(1 + \Delta S/2S) - \Delta H(1/S)(H - H_R + \Delta H/2) \tag{11}$$

In appendix A, it is shown that $|\eta_1|$ is less than 0.05 for any of the examples 1 through 3. It is further indicated that the increment:

$$\Delta\rho = \rho(\alpha[R + \Delta R], H + \Delta H) - \rho(\alpha R, H) \tag{12}$$

can be expressed in the form:

$$\Delta\rho = \Delta R(1 + \eta_2) - M(R/2b)\Delta H(1 + \eta_3) \tag{13}$$

where M = 0 when conversion error is controlled by the minimax method; M = 1 when

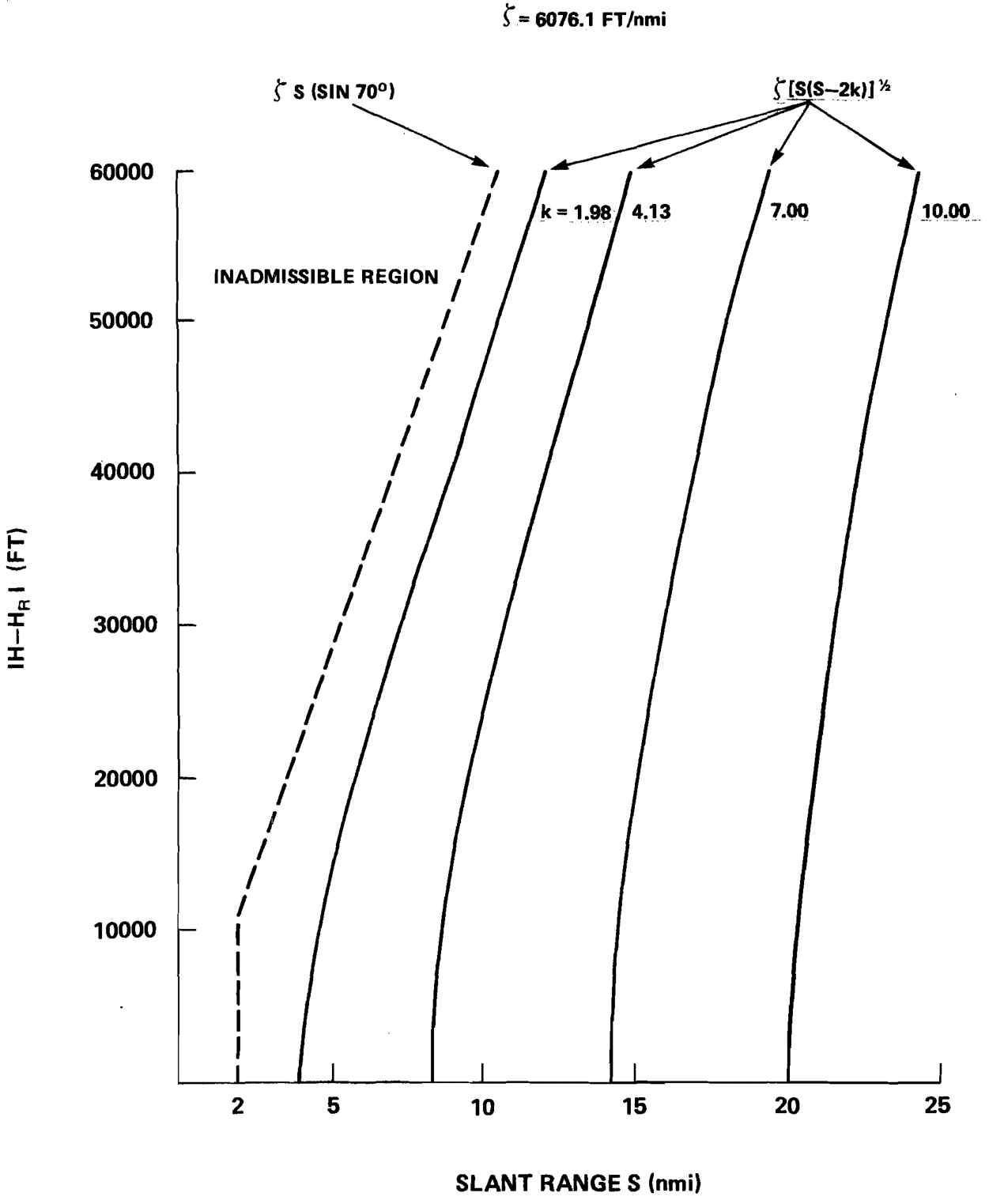

Figure 1. RESTRICTIONS ON REPORTED ALTITUDE AND SLANT RANGE MEASUREMENT

control is effected by the error correction technique. Moreover, as shown in appendix B, both $|\eta_2|$ and $|\eta_3|$ are less than 0.004 under the conditions cited in any one of the three examples. Finally, it is shown in appendix C that the increment:

$$\Delta z = z(\rho + \Delta\rho, \theta + \Delta\theta) - z(\rho, \theta) \tag{14}$$

can be expressed as:

$$\Delta z = (\Delta\rho - i\rho\Delta\theta)\epsilon^{i(\frac{\pi}{2} - \theta)}(1 + \eta_4) \tag{15}$$

where $|\eta_4|$ is bounded above by:

$$\ell(\Delta\theta) = \tan|\Delta\theta| + (1 + \tan|\Delta\theta|)(2 - \cos(\Delta\theta) - \sin(\Delta\theta)) \tag{16}$$

as long as $|\Delta\theta|$ is less than $\frac{\pi}{2}$ rad. The behavior of the function ℓ in the neighborhood of 0 is essentially that of $|\Delta\theta|$, as illustrated in figure 2.

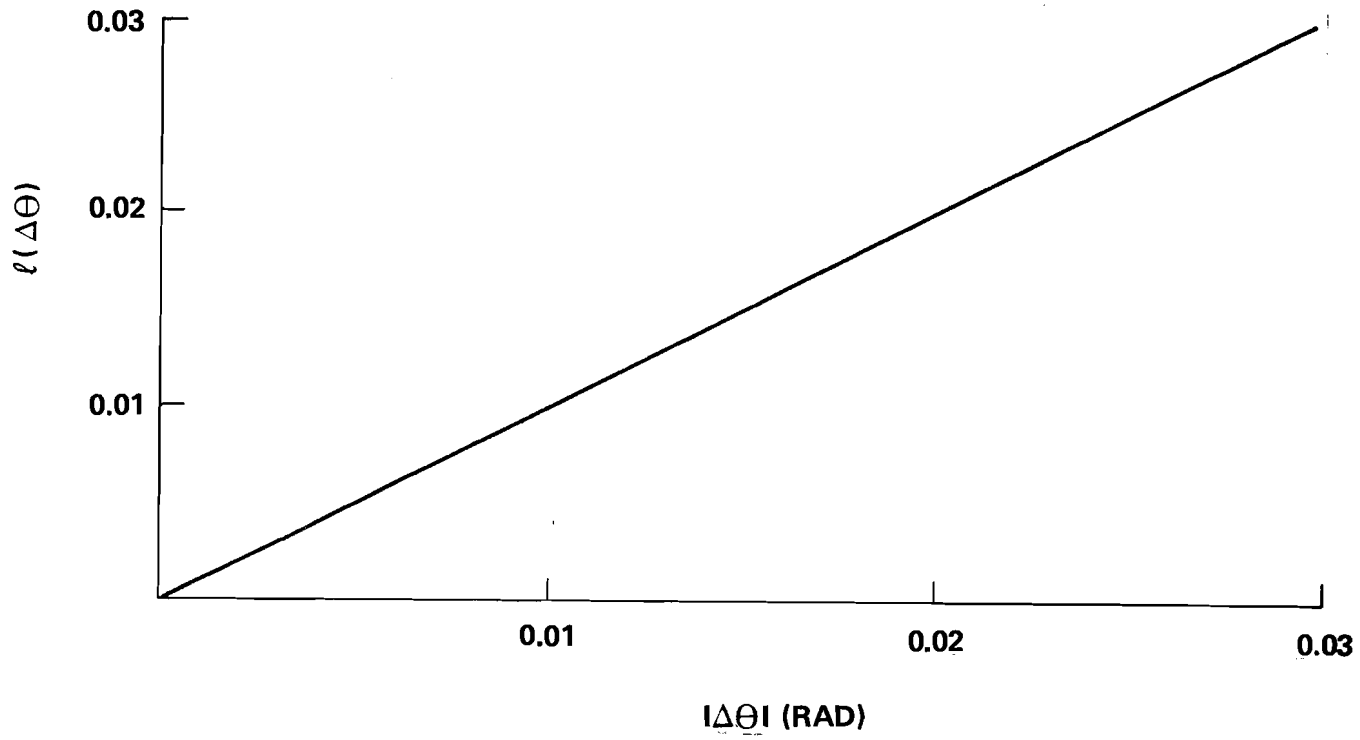

Figure 2. UPPER BOUND ON $|\eta_4|$

Based on the preceding remarks, it is apparent that Δz is accurately represented by the approximation:

$$\delta z = [(S/R)g - M(R/2b)\Delta H - i\rho\Delta\theta]\epsilon^{\,i(\frac{\pi}{2} - \theta)} \tag{17}$$

in examples 1 through 3. Under the constraints of section 2, and contingent on appendix B, it follows that:

$$\rho(\alpha R(S,H),H) = R(S,H)(1 + \eta_5) \tag{18}$$

where $|\eta_5|$ is less than 0.003 for any admissible point (S,H). Consequently, ρ in each example is interchangeable with R and does not introduce an appreciable change in the approximation error. The right side of (17) is a linear function of $\Delta\theta$. Based on the definition of g, it is essentially a linear function of $\Delta S(\Delta H)$ if $|S|/2S(|H|/2)$ is small compared to unity ($|H - H_R|$).

If $|w_o|$ is less than 1,000 nmi:

$$3357.9336 \text{ nmi} = E_o \leq E_r \leq a. \tag{19}$$

If $|z|$ does not exceed 200 nmi, and $|\Delta z|$ is less than 10 nmi (reference 1):

$$\Delta w = w(z + \Delta z) - w(z) = C\epsilon^{\,-i\beta\Delta z(1 + \eta_6)} \tag{20}$$

where:

$$|\eta_6| < 0.01 \tag{21}$$

and

$$C = E_r/E_s + |w_o|^2/4E_rE_s \tag{22}$$

(relationships (20) - (22) are valid regardless of whether w_z is defined by the right side of (7) or polynomial approximations thereof).

In the case of control region geometries of the type associated with air traffic control centers in NAS, the restrictions on E_r and $|w_o|$, and the requirements of sound design criteria regarding the structure of the master plane are easily met. It can be readily verified that the 200 nmi restriction on the ground range is immediately satisfied whenever the point (S,H) is admissible. Moreover, as shown in appendix C, $|\Delta z|$ is substantially less than 10 nmi under the conditions cited in the examples of the preceding section. Finally, it is true that:

$$0.975 = E_o/a \leq c \leq a/b + 10^6/4E_ob = 1.025 \tag{23}$$

under the restrictions cited above for E_r and $|w_o|$. Thus, (20) and (21) imply:

$$\Delta w = \epsilon^{\,-i\beta\Delta z(1 + \eta_7)} \tag{24}$$

where $|\eta_7|$ is less than 0.04.

In consideration of the preceding observations, approximation (17) in conjunction with either relation (20) or (24) provides a viable vehicle for estimating the impact of measurement errors on the representation of targets in the master plane. In the next section, these results are used to approximate second moments of the noise generated in the master plane by random measurement errors.

6. SECOND MOMENTS OF RANDOM FLUCTUATIONS IN THE MASTER PLANE

The parameter M equals either 0 or 1, depending on the method used to control the conversion error. Hereafter, w will denote the image of the datum (S,θ,H) in the master plane under the composition of mappings as described in section 3 in conjunction with the value assigned M. Additionally, the image of $(S+\Delta S,\theta+\Delta\theta,H+\Delta H)$ will be approximated under the same mapping by the sum of w and the increment:

$$\delta w = C(\delta\rho - i\, R\Delta\theta)\epsilon^{i(\frac{\pi}{2}-\gamma)} \tag{25}$$

where:

$$\delta\rho = (S/R)\Delta S - (h/R + MR/2b)\Delta H, \tag{26}$$

h represents the altitude $H - H_R$ above the radar, γ is the sum of the angles θ and β, and R denotes the square root of $S^2 - h^2$. The approximation (25) of the actual difference between the images of $(S+\Delta S,\theta+\Delta\theta,H+\Delta H)$ and (S,θ,H) is based on relationships (11), (17), and (20) under the assumption that $|\Delta S|/2S$ is small compared to unity and that $|h|$ is large relative to $|\Delta H|/2$.

If it is assumed that $\Delta S, \Delta\theta$, and ΔH are zero mean independent random variables with standard deviations σ_S, σ_θ, and σ_H, respectively, then the expected value of δw vanishes. Also, assuming $\sigma_1(\sigma_2)$ represents the standard deviation of the real (imaginary) part of δw, it can be shown that:

$$\sigma_1{}^2 = C^2[(\lambda_2 - \lambda_1)\sin^2\gamma + \lambda_1] \tag{27}$$

$$\sigma_2{}^2 = C^2[(\lambda_2 - \lambda_1)\cos^2\gamma + \lambda_1] \tag{28}$$

where:

$$\lambda_1(S,h) + (S^2 - h^2)\sigma_\theta{}^2 \tag{29}$$

$$\lambda_2(S,h) = (S^2 - h^2)^{-1}(S^2\sigma_S{}^2 + [h + M(S^2 - h^2)/2b]^2\sigma_H{}^2) \tag{30}$$

Likewise, it can be shown that the covariance σ_{12} of the real and imaginary parts of δw is expressed by:

$$\sigma_{12} = C^2[(\lambda_2 - \lambda_1)/2]\sin 2\gamma \tag{31}$$

and:

$$\rho_{32} = \sigma_{12}/\sigma_1\sigma_2 = [(\lambda_2 - \underline{\lambda}_1)/2]\sin 2\gamma/([(\lambda_2 - \underline{\lambda}_1)/2]^2\sin^2 2\gamma + \underline{\lambda}_1\underline{\lambda}_2)^{1/2} \quad (32)$$

is the corresponding correlation coefficient.

Clearly, the standard deviations of the real and imaginary parts of δw lie between $C\lambda_1^{1/2}$ and $C\lambda_2^{1/2}$. Moreover, $C\delta\rho$ can be conceived as the component of δw in the radial direction from the master plane representation w_o of the radar site to w, and $CR\Delta\theta$ can be treated as the cross-radial component in the direction of increasing azimuth (see section 7). In these random, uncorrelated variables $C\lambda_2^{1/2}$ and $C\lambda_1^{1/2}$ represent the standard deviations of the former and latter, respectively. Also, it is readily demonstrable that $\lambda_1(\lambda_2)$ decreases (increases) monotonically with increasing values of $|h|$ (h).

Thus, based on the definition:

$$\underline{h}(S) = \min [H_M, S \sin 70°] \quad (33)$$

it follows that:

$$\lambda_1(S,\underline{h}(S)) \leq \lambda_1(S,h) \leq \lambda_1(S,0) \quad (34)$$

$$\lambda_2(S,0) \leq \lambda_2(S,h) \leq \lambda_2(S,\underline{h}(S)) \quad (35)$$

whenever h lies in the closed interval $[0,\underline{h}(S)]$. In addition, for any h, it can be shown that:

$$\lambda_i(x,h) \sim \underline{\lambda}_i(x,o) \qquad (x \to \infty) \quad (36)$$

for i = 1 or 2, i.e.,

$$\lim_{x \to \infty} \lambda_i(x,h))/\underline{\lambda}_i(x,o) = 1 \quad (37)$$

These relationships are illustrated in figures 3 and 4 for both the ATCRBS and Mode S sensors. Note that λ_1 is independent of M, and figure 4 represents the case in which M = 1. If the bounds which form when M = 0 were plotted according to the scale of figure 4, the two would appear virtually identical. Thus, figure 4 is considered applicable to both cases. However, this does not mean that λ_2 is essentially invariant to M. Indeed, as x increases without bound, $\lambda_2(x,h)$ approaches σ_S^2 when M = 0, and it becomes arbitrarily large when M = 1.

As indicated in figures 3 and 4, λ_1 dominates λ_2 at large slant ranges. If M = 0, it can be shown that the condition $\lambda_1 \geq \lambda_2$ is equivalent to the requirement that the point (S,h) lie to the right of the locus on the equation:

$$S^2 = h^2 + (\sigma_S^2/2\sigma_\theta^2)\{1 + [1 + 4h^2(1 + \sigma_H^2/\sigma_S^2)(\sigma_\theta/\sigma_S)^2]^{1/2}\} \quad (38)$$

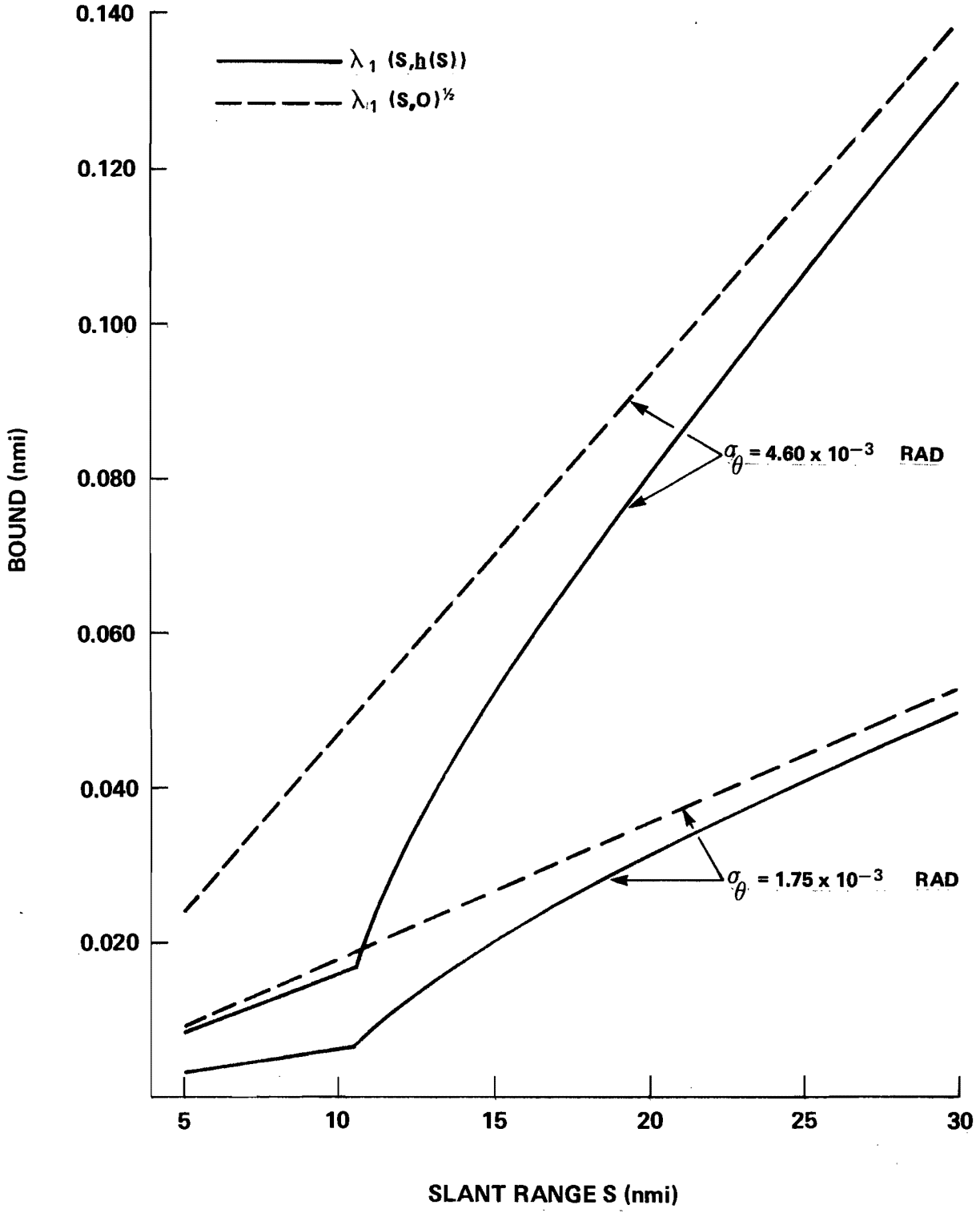

Figure 3. BOUNDS FOR STANDARD DEVIATION IN CROSS-RADIAL DIRECTION

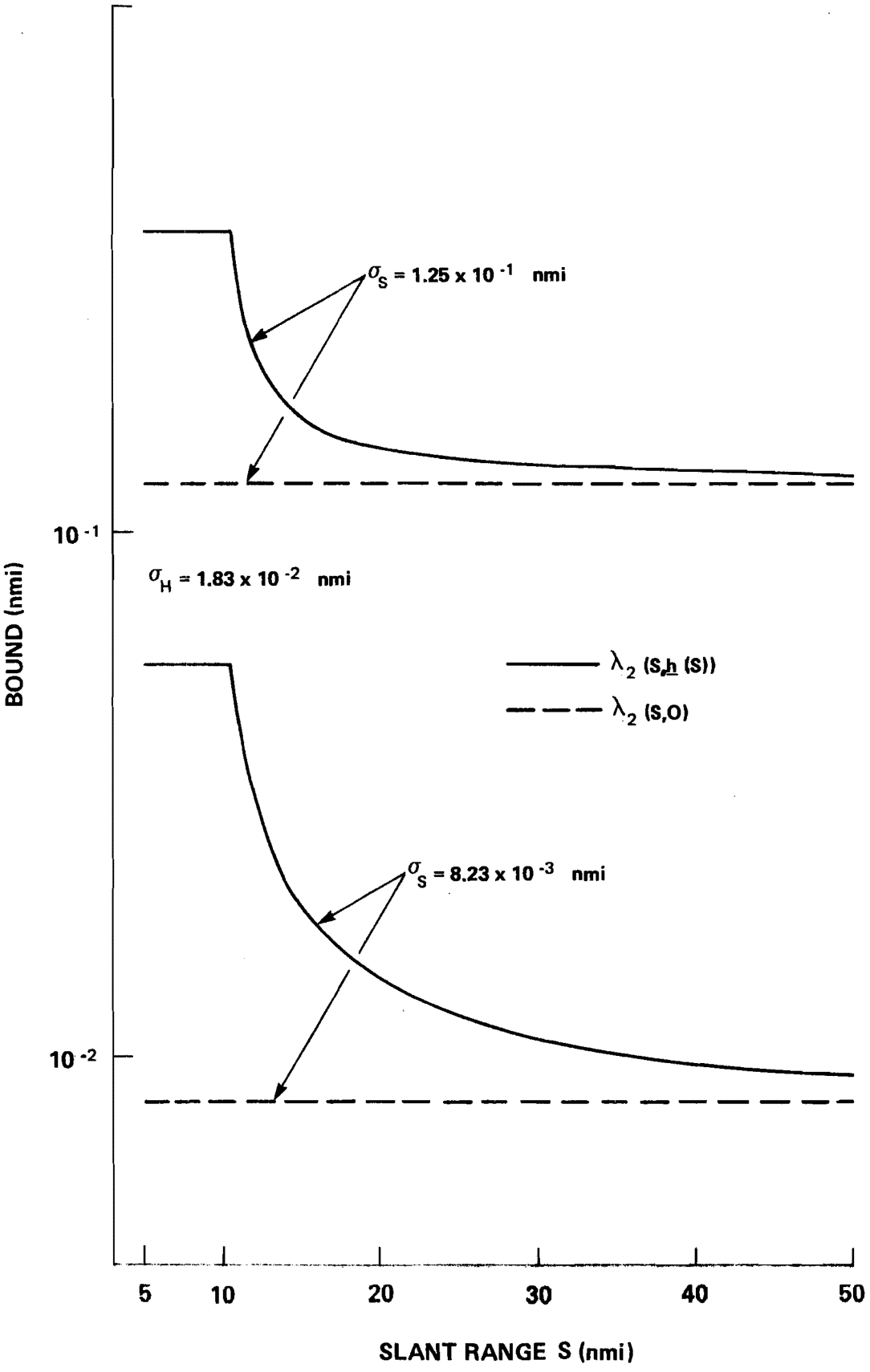

Figure 4. BOUNDS FOR STANDARD DEVIATION IN RADIAL DIRECTION

This is also essentially true when M = 1, provided that $h\sigma_H^2/b$ is much less than σ_S^2 and $\sigma_H^2/4b^2$ is much less than $\sigma^2\theta$. This is certainly the situation for the standard deviations cited in section 4 under the constraints of section 2. Figure 5 illustrates the locus of points (S,h) satisfying (39) for both the ATCRBS and Mode S sensors.

The absolute value of the correlation coefficient between the real and imaginary parts of δw is an increasing function of $|\sin 2\gamma|$ so that:

$$\hat{\rho}_{12} = \max_{0 \leq \alpha < 2\pi} |\rho_{12}| = |\lambda_2 - \lambda_1|/(\lambda_1 + \lambda_2) \tag{39}$$

Obviously, from (29) and (30), this is a function of the vector (S,h) and:

$$\hat{\rho}_{12}(x,h) \sim \rho_{12}(x,0) \quad (x \rightarrow \infty) \tag{40}$$

Suppose that $\lambda_2(S,0)$ is less than $\lambda_1(S,0)$. Then there exists a positive number $h_o(S)$ such that $\lambda_1(S,h_o(S))$ and $\lambda_2(S,h_o(S))$ are identical. Moreover, it can be shown that $\hat{\rho}_{12}(S,h)$ monotonically decreases to 0 as h increased through non-negative values to h_o (S) and thereafter becomes a monotonic increasing function of h. Contrarily, if $\lambda_2(S,0)$ is not less than $\lambda_1(S,0)$, then $\hat{\rho}_{12}(S,h)$ increases monotonically as h increases from 0. Hence, when h is a member of the interval $[0,\underline{h}(S)]$:

$$\hat{\rho}_{12}(S,h) \leq \max[\hat{\rho}_{12}(S,0), \hat{\rho}_{12}(S,h(S))] \tag{41}$$

and

$$\hat{\rho}_{12}(S,h) \geq \begin{cases} 0 & \text{if } h_o(S) \in [0,H_M] \\ \min[\hat{\rho}_{12}(S,0), \hat{\rho}_{12}(S,\underline{h}(S))] & \text{otherwise} \end{cases} \tag{42}$$

These bounds are illustrated in figures 6 and 7 for the case where M = 1. If the bounds for the case M = 0 are plotted to the same scale, the results are essentiallly reproductions of these figures.

Random fluctuations in the master plane cannot be presumed to be independent of altitude measurement errors. In particular, it is easy to verify that the correlation coefficient ρ_{1H} between ΔH and the real part of δw is given by:

$$\rho_{1H} = -(S^2 - h^2)^{-1/2}[h + M(S^2 - h^2)/2b]\sigma_H \sin\gamma / [(\lambda_2 - \lambda_1)\sin^2\gamma + \lambda_1]^{1/2} \tag{43}$$

The correlation coefficient ρ_{2H} between H and the imaginary part of δw can be

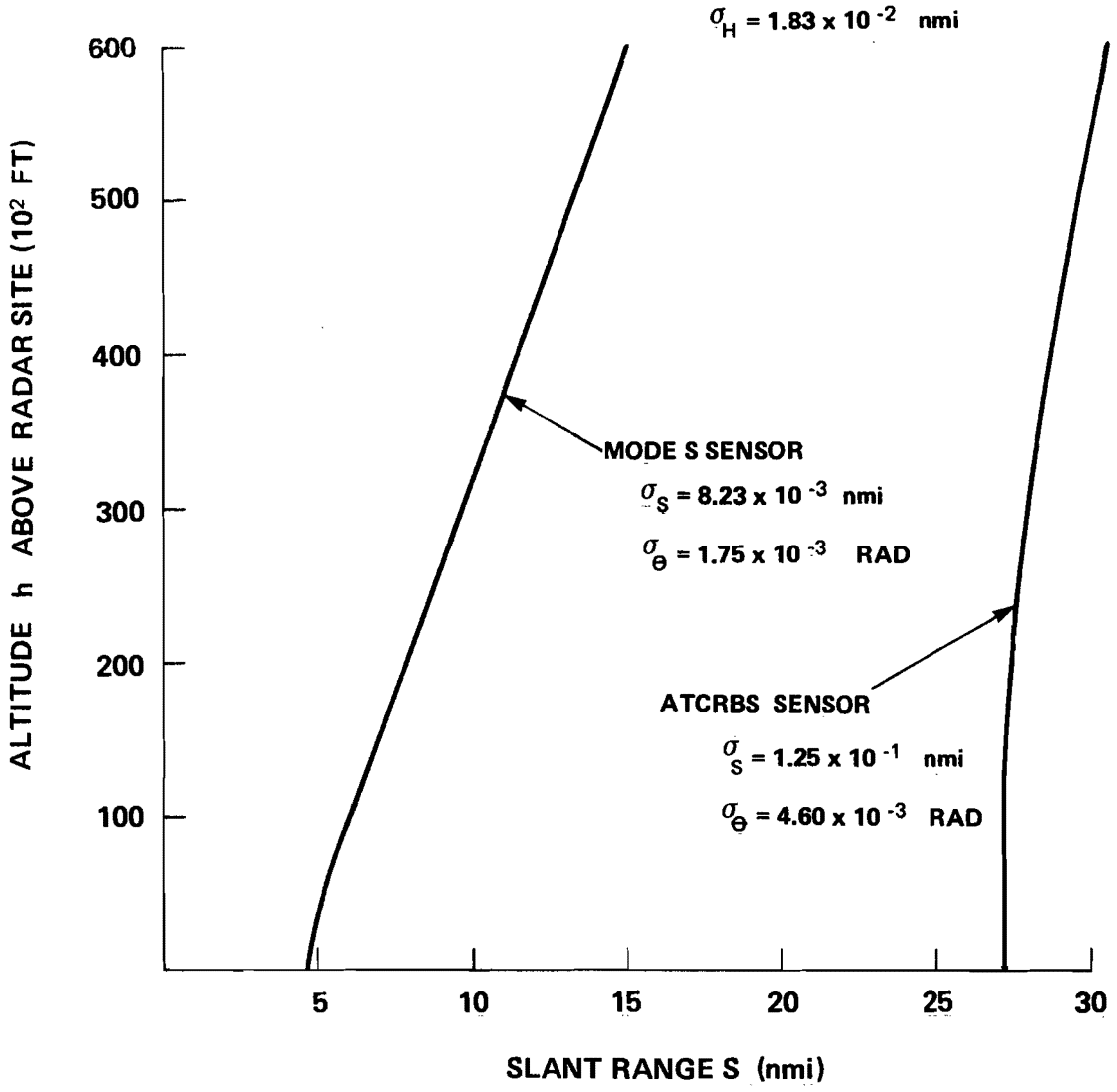

Figure 5. LOCUS OF POINTS (S,h) FOR WHICH $\lambda_1 = \lambda_2$

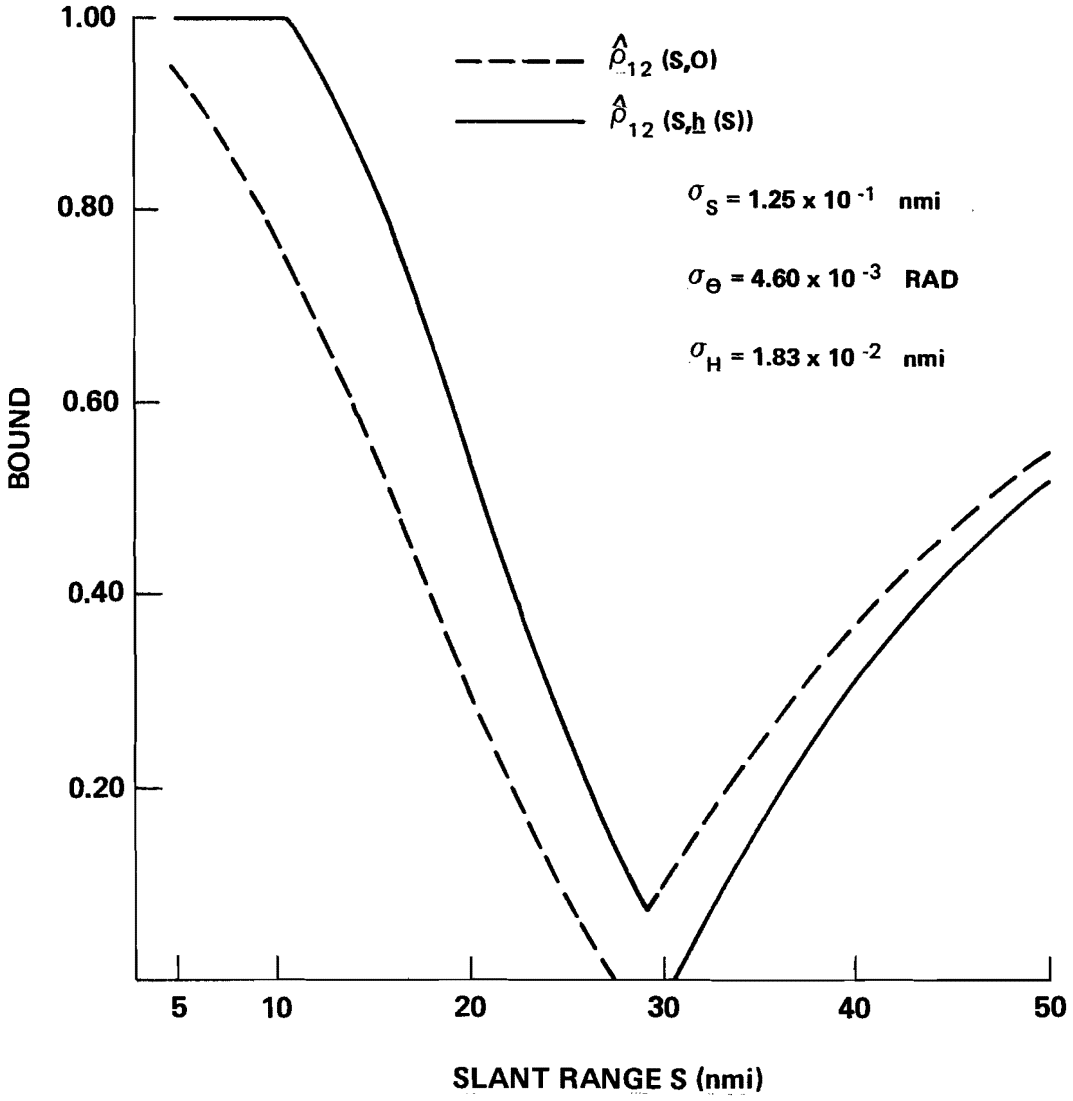

Figure 6. BOUNDS ON CORRELATION BETWEEN REAL AND IMAGINARY PARTS OF δw FOR ATCRBS SENSOR

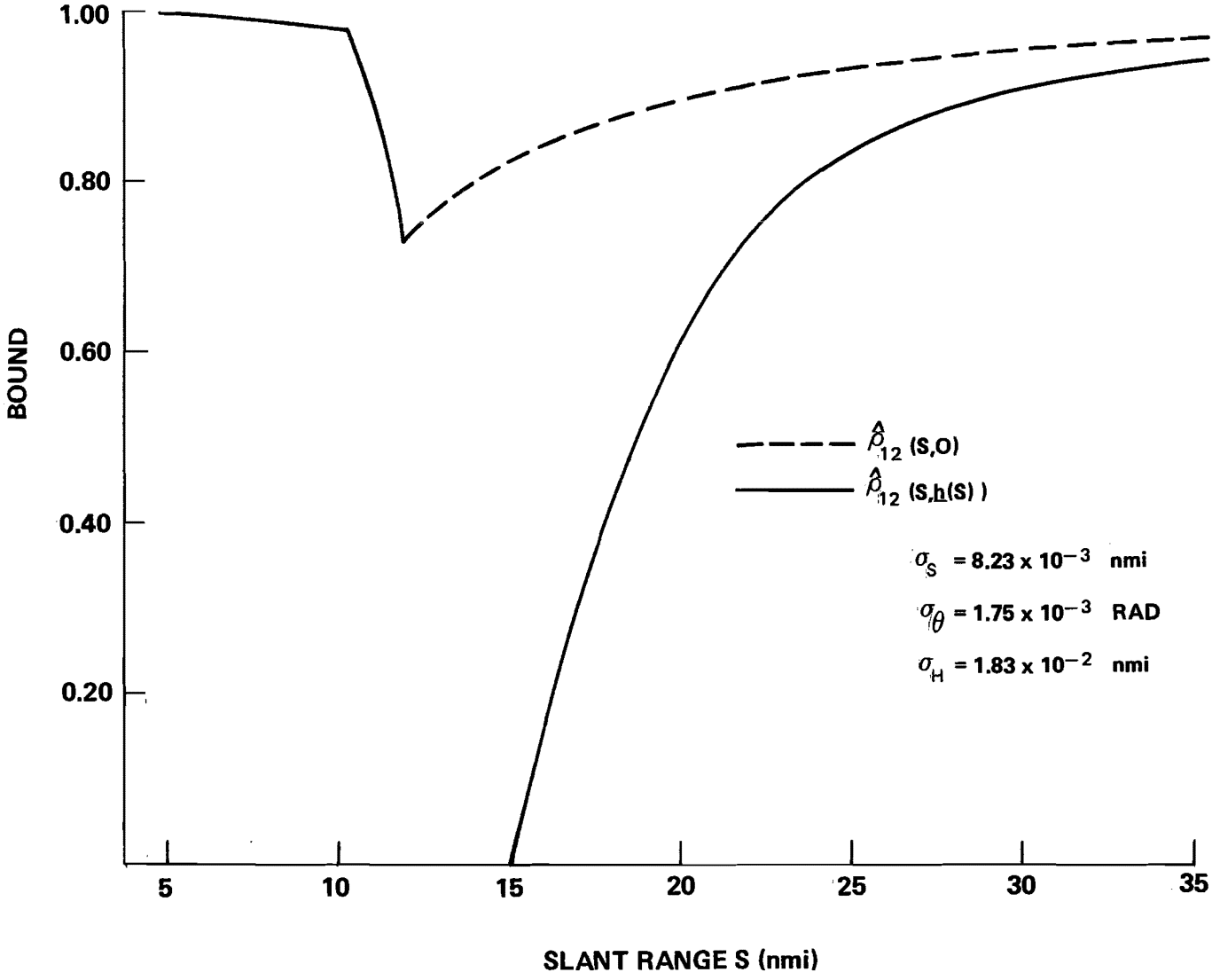

Figure 7. BOUNDS ON CORRELATION BETWEEN REAL AND IMAGINARY PARTS OF δw FOR MODE S SENSOR

obtained from this expression by replacing sin γ with cos γ . Moreover, it can be verified that:

$$\hat{\rho} = \max_{0 \le \gamma < 2\pi} |\rho_{1H}| = \max_{0 \le \gamma \le 2\pi} |\rho_{2H}| = (S^2-h^2)^{-1/2}[h+M(S^2-h^2)/2b]\sigma_H/\lambda_2^{1/2} \tag{44}$$

This, of course, is a function of (S,h), with the result:

$$\hat{\rho}(x,h) \sim \hat{\rho}(x,0) \qquad (x \to \infty) \qquad \text{if } M = 1 \tag{45}$$

$$\lim_{x \to \infty} \hat{\rho}(x,h) = \hat{\rho}(x,0) = 0 \qquad \text{if } M = 0 \tag{46}$$

Moreover, it can be shown that $\hat{\rho}(S,h)$ increased monotonically as h increases from 0. Consequently, when h is in $[0,\underline{h}(S)]$:

$$\hat{\rho}(S,0) \le \hat{\rho}(S,h) \le \hat{\rho}(S,\underline{h}(S)) \tag{47}$$

In the case where M = 1, the lower bound $\hat{\rho}(S,0)$ is a monotonic increasing function of S with limit 1. However, at a slant range of 200 nmi it is less than 0.0043 (0.065) for the ATCRBS (Mode S) sensor. The upper bound is illustrated in figure 8 for the case where M is unity.

7. CONFIDENCE REGION

We define Σ to be the covariance matrix of the real and imaginary parts of δw, i.e.,

$$\Sigma = \begin{bmatrix} \sigma_1^2 & \sigma_{12} \\ \sigma_{12} & \sigma_2^2 \end{bmatrix} \tag{48}$$

Letting I represent the identity matrix, the eigenvalues of Σ are the solutions of the quadratic equation in λ obtained by setting the determinant of the difference between Σ and λI equal to zero. The solutions are $C^2\lambda_1$ and $C^2\lambda_2$, and, of course, the determinant of Σ is the product of these solutions. Since λ_1 and λ_2 are nonzero for any admissible point (S,H), it is clear that Σ^{-1} exists. Moreover, as the inverse of a covariance matrix, it must be positive definite.

Assume that $\overline{w}$ denotes the column matrix $[w_1,w_2]^T$ where w_1 (w_2) represents the real (imaginary) part of w and T denotes the transpose of a matrix. Also, corresponding to any positive number p, is defined U(p) as the set of all column matrices:

$$\overline{x} = [x_1,x_2]^T \tag{49}$$

such that:

$$[\overline{x} - \overline{w}]^T \Sigma^{-1} [\overline{x} - \overline{w}] \le p \tag{50}$$

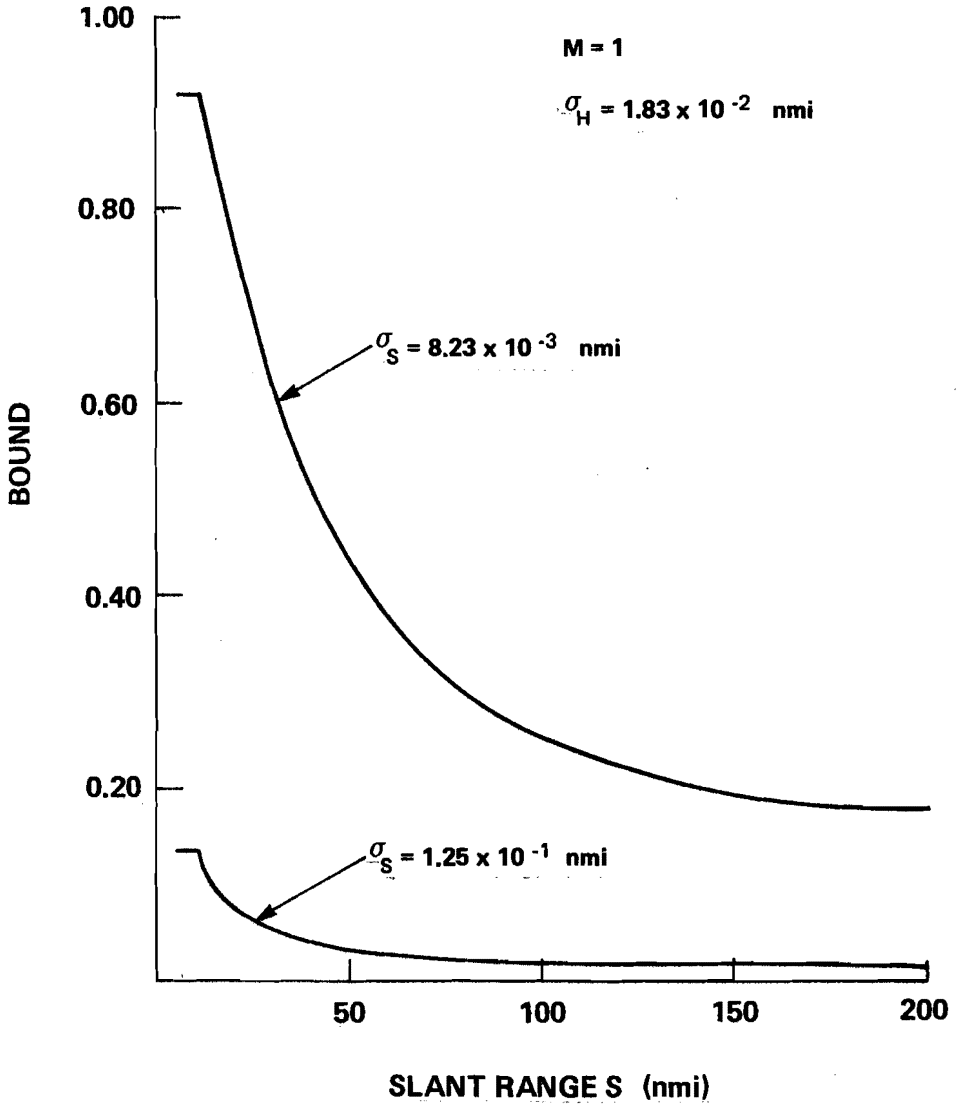

Figure 8. UPPER BOUND $\hat{\rho}(S,h(S))$ ON CORRELATION BETWEEN ALTITUDE ERROR ΔH AND REAL (IMAGINARY) PART OF δw

It can be shown that U(p) is equivalent to a region of the master plane bound by an ellipse centered at w. In fact, as shown in figure 9, one axis of the ellipse lies on the line

$$x_2 - w_2 = (\cot \gamma)(x_1 - w_1) \tag{51}$$

when γ is not equal to an integer multiple of π. When γ is 0 or π, it lies on the line through w parallel to the imaginary axis. In either case, the half length of this axis of the ellipse is $C(p\lambda_2)^{1/2}$. The half-length of the remaining axis is $C(p\lambda_1)^{1/2}$.

Note that figure 9 depicts one axis of the ellipse as a segment of the line passing through w and w_o, the master plane representation of the radar site. This depiction is actually an approximation of the fact. Under the constraints listed in section 5 for E_r, $|w_o|$, and $|z|$, it can be shown from relations (3) and (7) that:

$$w - w_o = c\rho\epsilon^{\,i(\frac{\pi}{2} - \gamma)}\,(1+\eta_8) \tag{52}$$

where $|\eta_8|$ is less than 0.005. To this extent, $w-w_o$ can be conceived as a directed line segment forming an angle γ with the imaginary axis of the master plane. Additionally, (18) and (52) provide some justification for interchanging ρ, R_1 and $|w_1-w_o|/C$. A cursory examination of section 6 reveals that this permits the approximating of the statistical properties of noise in the master plane in terms of $|w-w_o|$, γ, and h instead of S, γ, and h.

Suppose that ΔS, $\Delta\theta$, and ΔH are normally distributed. It follows that the real and imaginary parts of δw have a bivariate normal distribution. As a result,

$$P = 2\pi C^{-2}(\lambda_1\lambda_2)^{-1/2} \int_{U(p)} \exp[-(\bar{x}-\bar{w})^T \Sigma^{-1}(\bar{x}-\bar{w})/2]d\bar{x} \tag{53}$$

is the probability that the random variable $w+\delta w$ will lie in the set U(p). Letting:

$$\bar{y} = \sqrt{\Sigma}^{-1}(\bar{x}-\bar{w}) \tag{54}$$

where $\sqrt{\Sigma}$ denotes the usual square root of the positive definite matrix Σ, it follows that:

$$P = (1/2\pi) \int_{||\bar{y}||^2 \leq p} \exp[-||\bar{y}||^2/2]d\bar{y} = 1 - \exp(-p/2) \tag{55}$$

Thus, p is a measure of the probability P. Conversely, the area A of the region U(p) is given by:

$$A = \pi p C^2(\lambda_1\lambda_2)^{1/2} \tag{56}$$

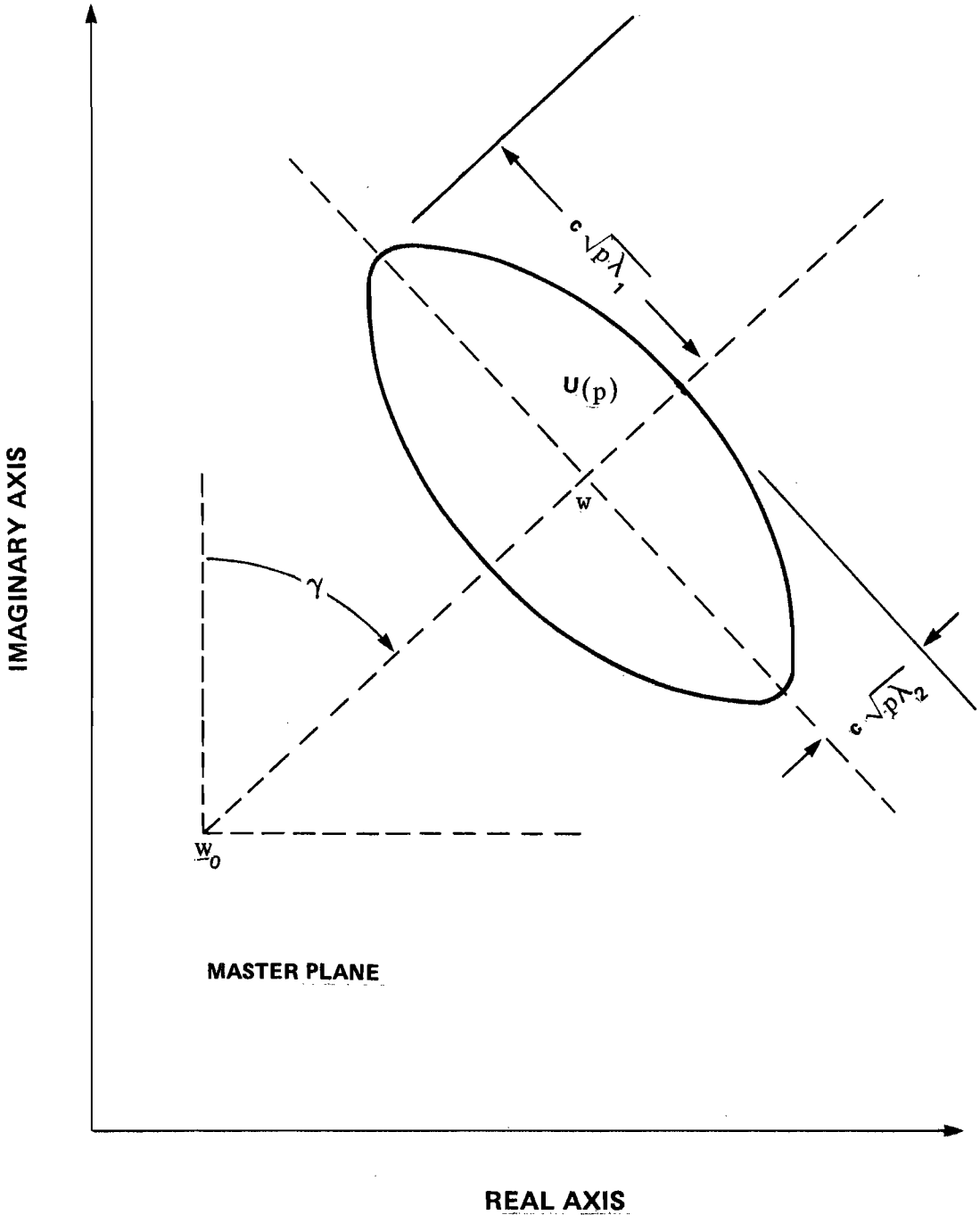

Figure 9. ELLIPTICAL CONFIDENCE REGION

Consequently, if the elliptical region illustrated in figure 9 is to serve as a confidence set for $w+\delta w$ at a prescribed confidence level P, then the area of the set must vary with the datum (S,θ,H) in accord with the relationship:

$$A = \pi[-2\ \ln(1-P)]C^2(\lambda_1\lambda_2)^{1/2} \tag{57}$$

This, of course, is the basis for the so-called dynamic search area concept in tracking (reference 4).

Clearly, the product:

$$A_0 = \pi(\lambda_1\lambda_2)^{1/2} \tag{58}$$

is a function of the vector (S,h) and

$$A_0(x,h) \sim A_0(x,0) \qquad (x \rightarrow \infty) \tag{59}$$

Moreover, it can be verified that $A_0(S,h)$ increases monotonically as h increases from 0. Hence,

$$A_0(S,0) \leq A_0(S,h) \leq A_0(S,\underline{h}(S)) \tag{60}$$

as long as h is an element of the closed interval $[0,\underline{h}(S)]$. These bounds are illustrated in figure 10 for the case where M = 1. Note that the difference between the bounds for the ATCRBS sensor is not readily apparent when contrasted against the scale of figure 10; therefore, the corresponding lower bound does not appear as a separate curve in the illustration. With deference to the preceding remarks concerning the dependence of λ_1, and λ_2, upon M, it can be inferred that figure 10 is also a fairly accurate representation of the case where M = 0.

8. CONCLUDING REMARKS

Consideration has been afforded the linear approximations of the effects of errors in the measurement of slant range, azimuth, and altitude on planar representations of targets in the en route ATC environment. Approximations have been quantified to conform with current and projected application of sensor measurements to the control function. The linear formulation will provide an approximate representation of the effects of measurement errors on the location of targets with respect to the master plane coordinate system for all targets which are neither geographically nor altitudinally adjacent to the radar. Applications include the characterization of errors at the input to tracking filters due to random and/or trend-like phenomena.

In this report, the approximations have been used in a statistical characterization of fluctuations induced in the master plane by random measurement errors consistent with noise levels commonly associated with the ATCRBS and Mode S sensors. In general, the covariance matrix of the Cartesian components of these fluctuations depend upon reported altitude and measurements of slant range and azimuth.

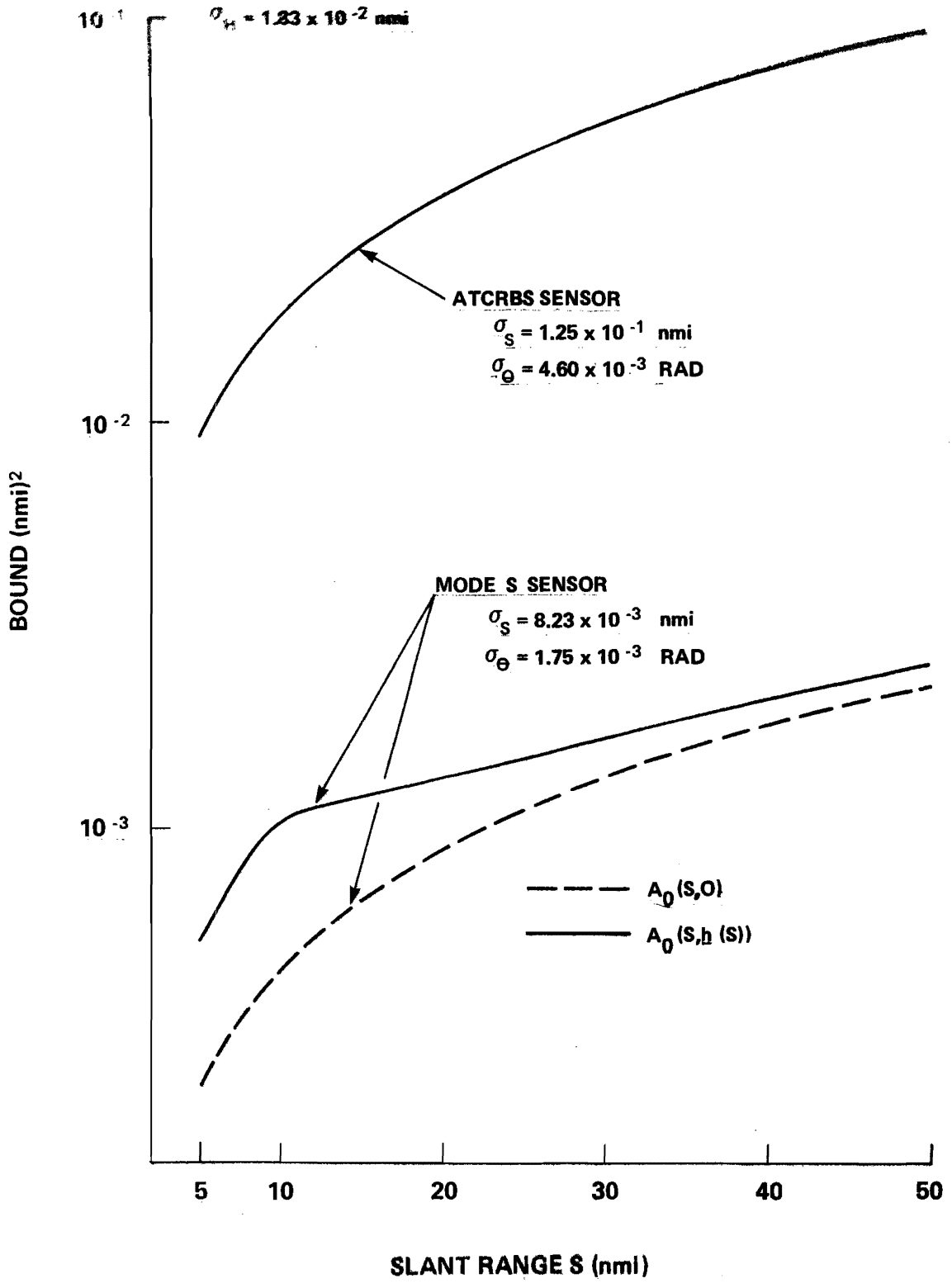

Figure 10. NORMALIZED SIZE OF CONFIDENCE REGION

However, with increasing slant range, it asymptotically approaches a matrix function that is invariant to altitude. Thus, at large slant ranges (in excess of 50 nmi) the covariance matrix is essentially invariant with respect to altitude under typical operating conditions. However, at lesser ranges, the variation of second moments with altitude can be significant. Similar observations apply to the size of confidence regions for target locations.

9. REFERENCES

1. R. Mulholland and D. Stout, Numerical Studies of Conversion and Transformation in a Surveillance System Employing a Multitude of Radars - Parts I and II. ADA 072 085 and ADA 072 086, NTIS, April 1979.

2. A Mundra, General Aviation Altimetry Errors for Collision Avoidance Systems, Journal of the Institute of Navigation, Winter 1979 - 80.

3. R. Rigolizzo, One-day Collection of Aircraft Altitude Data at Fort Huachuca, Arizona, Technical memo, April 1980.

4. R. Lefferts, Calculation of the Correlation Region Size for Use with Alpha-Beta Tracking Filters, ADA 072 083, NTIS, April 1979.

APPENDIX A

INCREMENT IN R

For the moment, let us consider the function R defined by (2) for all (S,H) satisfying the condition:

$$S \geq |H - H_R| \geq 0 \tag{A1}$$

Also, let us define e to be the product of:

$$f = 2S/R(S,H)^2 \tag{A2}$$

and g where the latter is given by (11). Then the increment ΔR defined by (9) can be expressed as:

$$\Delta R = R(S,H)(e/2)\ [1 + \delta(e)] \tag{A3}$$

where:

$$\delta(e) = \begin{cases} 0 & \text{if } e = 0 \\ (2/e)[(1 + e)^{1/2} - e/2 - 1] & \text{if } e \neq 0 \end{cases} \tag{A4}$$

The function $\delta(e)$ represents the relative error incurred through use of the approximation:

$$\delta R = [S/R(S,H)]g \tag{A5}$$

It can be shown that $|\delta(e)|$ cannot exceed $\delta(-|e|)$ in the range where $|e|$ is less than 1. Figure A1 illustrates the accuracy of the approximation as e approaches 0.

It can be shown that the inequality:

$$f \leq 1/k \tag{A6}$$

is equivalent to (8) for all $k > 0$. Consequently, as illustrated in figure 1, the points $(S,H-H_R)$ for which:

$$|e| \leq |g|\ /k \tag{A7}$$

lie on and below the locus of those points for which the right and left sides of (8) are equal. Moreover, it can be verified that:

$$|g| \leq \begin{cases} 0.75 \text{ nmi} & \text{in example } 1 \\ 0.36 \text{ nmi} & 2 \\ 1.19 \text{ nmi} & 3 \end{cases} \tag{A8}$$

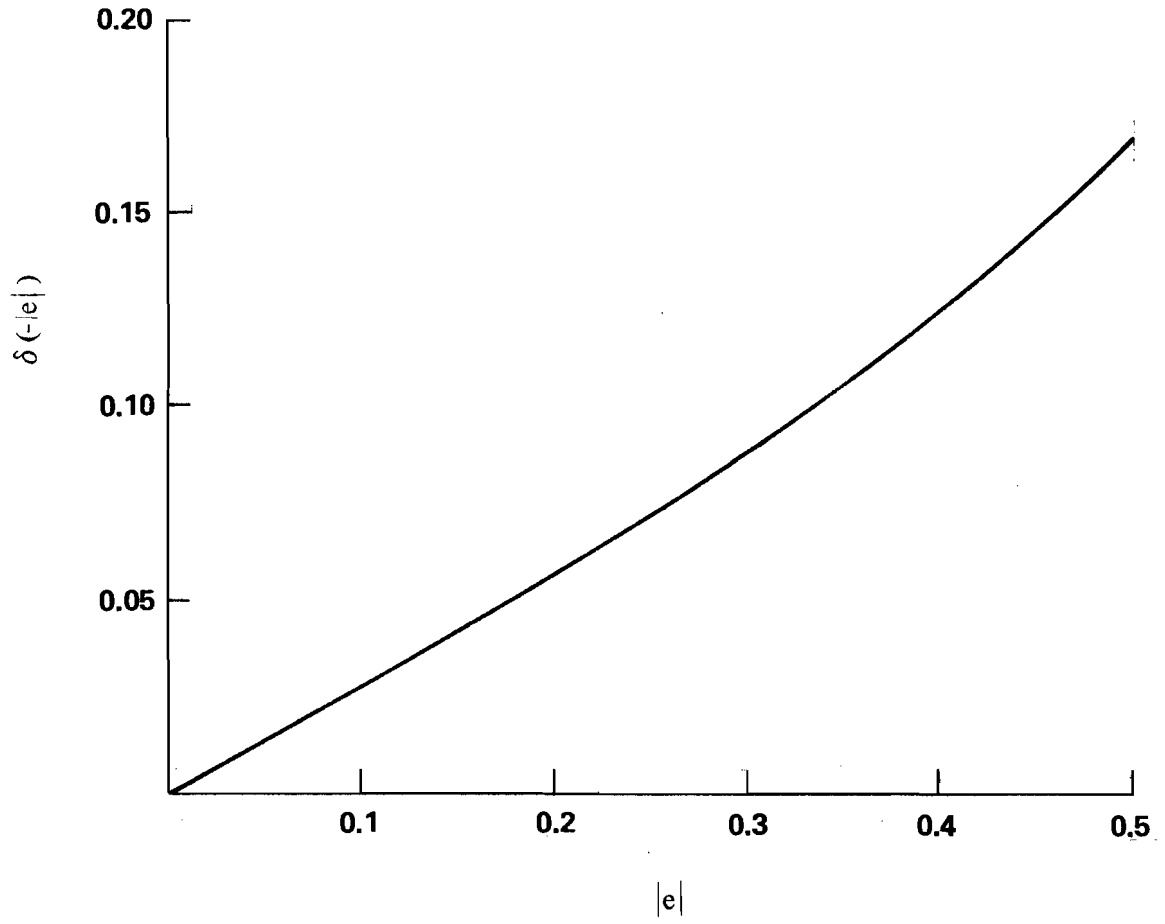

Figure A1. RELATIVE ERROR DUE TO APPROXIMATION OF THE INCREMENT ΔR.

Thus, in example 3, $|e|$ is less than 0.170 (1.19/7), thus implying that $\delta(e)$ is less than 0.05. Similarly, in example 1 (example 2) it can be shown that $\delta(e)$ is less than 0.05. Note that e must exceed -1. Otherwise:

$$|S + \Delta S| \leq |H + \Delta H - H_R|, \tag{A9}$$

and $R(S+\Delta S, H+\Delta H)$ is zero or imaginary contrary to the definitions of R in accord with (A1). Therefore, the condition:

$$|\Delta R|/R = |(e/2)[1+\delta(e)]| = |(1+e)^{1/2} - 1| \leq 1 \tag{A10}$$

is equivalent to:

$$-1 < e \leq 3 \tag{A11}$$

which is certainly the case in examples 1-3. Finally, if (S,H) is admissible, then:

$$R(S,H)|e|/2 = [1-(H-H_R)^2/S^2]^{-1/2}|g| \leq (\cos 70°)^{-1}|g| \tag{A12}$$

Thus, when (S,H) is admissible, $|\Delta R|$ is less than 10 nmi if:

$$1+|\delta(e)| < 10 \cos 70°/|g| \tag{A13}$$

Obviously, this condition is satisfied in examples 1-3. Indeed, $|\Delta R|$ is less than 3-7 nmi in all three examples.

APPENDIX B

INCREMENT IN ρ

In the case of the minimax procedure, the increment (12) can be expressed as:

$$\Delta\rho = \alpha\Delta R \tag{B1}$$

Under the constraints of section 2,

$$0.9989 = \alpha(b,H_R') \leq \alpha(E_s,H_R) \leq \alpha(a,0) = 0.9993 \tag{B2}$$

where H_R' represents the upper bound of 1.646 nmi imposed upon the altitude of the radar site.

When the error correction technique is employed:

$$\Delta\rho = \Delta R(1+\delta_1) - (R/2b)\Delta H(1+\delta_2) \tag{B3}$$

where:

$$1+\delta_1 = 2\alpha-\alpha\beta+ \alpha^3\beta 3R^2(1+\Delta R/R+\Delta R^2/3R^2)/8b^2-\alpha\beta(H+\Delta H)/2b \tag{B4}$$

$$1+\delta_2 = \alpha\beta \tag{B5}$$

and β represents the inverse of the square root of 1+K/b. Using the data supplied in sections 2 and 3, β is 0.9985 and R (S,H) cannot exceed 200 nmi for an admissible point (S,H). Moreover, as shown in appendix A, the ratio $|\Delta R|/R$ is not greater than 1 under the conditions cited in examples 1-3. It follows that both $|\delta_1|$ and $|\delta_2|$ are less than 0.004 for each of the three examples.

APPENDIX C

INCREMENT IN z

Suppose z is the complex valued function of the real variables ρ and θ defined by (3) for all ρ greater than 0. Then, if $|\Delta\theta| \leq \pi$, the increment (14) can be expressed as:

$$\Delta z = \epsilon^{i(\frac{\pi}{2} - \theta)} \left[\Delta\rho(1+\delta_1) - i\rho\Delta\theta(1+\delta_2)\right](1+\delta_3) \tag{C1}$$

where:

$$\delta_1 = \cos\Delta\theta - 1 \tag{C2}$$

$$\delta_2 = \sin\Delta\theta - 1 = \begin{cases} 0 & \text{if } \Delta\theta = 0 \\ \sin\Delta\theta/\Delta\theta - 1 & \text{otherwise} \end{cases}$$

$$\delta_3 = \begin{cases} 0 & \text{if } \Delta\theta = \Delta\rho = 0 \\ [\cos\Delta\theta - 1 - i(\Delta\rho/\rho)\sin\Delta\theta][(\Delta\rho/\rho)\cos\Delta\theta - i\Delta\theta\sin\Delta\theta]^{-1} & \text{otherwise} \end{cases} \tag{C3}$$

This expression can be rewritten in the form (15) where:

$$\eta_4 = \begin{cases} 0 & \text{if } \Delta\theta = \Delta\rho = 0 \\ \delta_3 + (1+\delta_3)(\Delta\rho\delta_1 - i\rho\Delta\theta\delta_2)(\Delta\rho - i\rho\Delta\theta)^{-1} & \text{otherwise} \end{cases} \tag{C4}$$

clearly,

$$|\eta_4| \leq |\delta_3| + (1+|\delta_3|)(|\delta_4| + |\delta_2|) \tag{C6}$$

In addition, assuming $|\Delta\theta|$ does not exceed $\frac{\pi}{2}$, it can be shown that $|\delta_3|$ is an increasing function of either of the two variables $|\Delta\rho|/\rho$ and $|\Delta\theta|$ and:

$$\lim_{\Delta\rho/\rho \to \infty} |\delta_3| = \tan|\Delta\theta| \tag{C7}$$

As a result, $|\eta_4|$ is bound above by (16).